LEVEL II

ADA062258

Time Dependent Studies of Reactive Shocks in the Gas Phase

E.S. ORAN, T.R. YOUNG and J.P. BORIS

Laboratory for Computational Physics

November 16, 1978

D D C

RECEIVED

DEC 18 1978

D

NAVAL RESEARCH LABORATORY
Washington, D.C.

78 12 11 024

REPORT DOCUMENTATION PAGE		READ INSTRUCTIONS BEFORE COMPLETING FORM
1. REPORT NUMBER NRL Memorandum Report 3889	2. GOVT ACCESSION NO.	3. RECIPIENT'S CATALOG NUMBER
4. TITLE (and Subtitle) TIME DEPENDENT STUDIES OF REACTIVE SHOCKS IN THE GAS PHASE		5. TYPE OF REPORT & PERIOD COVERED Interim report on a continuing NRL problem.
		6. PERFORMING ORG. REPORT NUMBER
7. AUTHOR(s) E. S. Oran, T. R. Young, and J. P. Boris		8. CONTRACT OR GRANT NUMBER(s)
9. PERFORMING ORGANIZATION NAME AND ADDRESS Naval Research Laboratory Washington, D.C. 20375		10. PROGRAM ELEMENT, PROJECT, TASK AREA & WORK UNIT NUMBERS NRL Problem C01-15 ONR Project RR024-02-41 61153N-24
11. CONTROLLING OFFICE NAME AND ADDRESS Office of Naval Research Arlington, Virginia 22217		12. REPORT DATE November 16, 1978
		13. NUMBER OF PAGES 41
14. MONITORING AGENCY NAME & ADDRESS(if different from Controlling Office)		15. SECURITY CLASS. (of this report) UNCLASSIFIED
		15a. DECLASSIFICATION/DOWNGRADING SCHEDULE

16. DISTRIBUTION STATEMENT (of this Report)

Approved for public release; distribution unlimited.

17. DISTRIBUTION STATEMENT (of the abstract entered in Block 20, if different from Report)

18. SUPPLEMENTARY NOTES

19. KEY WORDS (Continue on reverse side if necessary and identify by block number)

Shocks
Reactive flow
Hydrogen Combustion
Detonations

20. ABSTRACT (Continue on reverse side if necessary and identify by block number)

The coupling of the hydrodynamics and the chemical kinetics in a reactive mixture ignited by the passage of a shock is examined using a time-dependent numerical model. The fluid dynamic and chemical rate equations are integrated self-consistently on their own characteristic time-scales using the flux-corrected transport and selected asymptotic methods, respectively. Results are presented for a shock in an H_2-O_2 mixture. The detailed calculations of the chemical and fluid structure of the shocked region show clearly how the chemical energy released is partitioned

(Continues)

DD FORM 1473 EDITION OF 1 NOV 65 IS OBSOLETE
1 JAN 73
S/N 0102-014-6601

20. Abstract (Continued)

between the fluid motion and the internal energy. A calculation is also shown for a reactive shock reflected from a rigid wall.

LEVEL II

ACCESSION for

DTIC	White Section	X
SMS	Buff Section	☐
UNANNOUNCED		☐
JUSTIFICATION		

BY
DISTRIBUTION/AVAILABILITY CODES

| Dist. | AVAIL, and/or SPECIAL |
| A | |

D D C

RECEIVED
DEC 18 1978
D

CONTENTS

TIME DEPENDENT STUDIES OF REACTIVE SHOCKS
IN THE GAS PHASE

I. Introduction

This paper presents results obtained from a detailed numerical simulation model designed to aid in theoretical and experimental studies of shock and detonation phenomena. The calculations describe the non-equilibrium chemical kinetics, reaction products, and intermediates produced in reactive gas mixtures ignited by the propagation of a shock front. The model is based on a rather general, compressible, one-dimensional reactive flow model designed to treat multi-fluid problems. Since the fluid dynamics and the chemical kinetics are time-dependent and self-consistent, we can observe the effects of the chemical energy release on the fluid flow during highly exothermic reactions and the effects of temperature and density inhomogeneities in the reaction medium on the resulting chemical composition.

In order to illustrate one type of physical problem which the reactive shock model can address, we simulate a shock tube in which a diaphragm is burst at the onset of the calculation. We assume that initial temperatures have equilibrated across the diaphragm which separates regions of differing pressures. The calculational method discussed below has first been tested against the results obtained from a derivation of the shock parameters in an ideal gas with no conductivity, diffusion, or chemical kinetics. We then proceed to examine a shock propagating in an H_2-O_2 medium. The detailed kinetics are confined to this relatively simple combustion process since it has been studied extensively using shock tube as well as flame-structure experiments. We look in detail at two reactive flow cases: one in which the chemical energy is released quickly enough to alter the properties of the shock, and the second in which the shock

is reflected from a rigid wall. We look behind the shock as it reflects off the end wall and observe the increased temperature and reaction products.

In the sections that follow, the numerical algorithms which are the foundation of the fluid transport and chemical integration are described, followed by a description of the chemical reaction scheme and the physical processes included in the model. In Section IV several calculations are described. The initial evolution of a shock propagating in an H_2-O_2 mixture with and without chemical reactions is compared to calculations performed in gas mixtures where fluid dynamic motion is suppressed. The later evolution of the reactive shock is also presented as the shock reflects from a rigid wall.

Before proceeding, however, it is useful to put this model and the sample calculation in perspective with other types of calculations used for shock and detonation studies. First, this is a time-dependent model, but not a time-dependent kinetics or hydrodynamic calculation alone; special emphasis has been placed on the precise coupling of these interactions. Thus the model is used to study transient phenomena, the approach to steady state, the way in which a perturbation on the system alters the steady state, the effects of non-ideality of gases, and the way in which the release of chemical energy alters flow patterns. Because the algorithm used to solve the hydrodynamics has minimal numerical diffusion and no artificial viscosity, a gradient as steep as a shock front can be resolved in one or two cells. Thus the model could, for example, be used to perform detailed, time-dependent simulations of how the shape of the shock front can be altered by endothermic,

2

exothermic, or relaxation processes. In summary, the major advance we are describing is the application of extremely accurate, efficient state-of-the-art numerical techniques to the study of the interplay between fundamental flow and chemical processes.

II. Numerical Model

We solve the time-dependent equations for conservation of mass, momentum, and energy:

$$\frac{\partial \rho}{\partial t} = - \nabla \cdot \rho \, \underline{v} \tag{1}$$

$$\frac{\partial \rho_i}{\partial t} = - \nabla \cdot \rho_i \underline{v} - \nabla \cdot \rho_i \underline{V}_i + P_i - L_i \rho_i \tag{2}$$

$$\frac{\partial \rho \underline{v}}{\partial t} = - \nabla \cdot \rho \, \underline{v} \, \underline{v} - \underline{\nabla} P + \nabla \cdot \eta \, \underline{\nabla} \, \underline{v} \tag{3}$$

$$\frac{\partial E}{\partial t} = - \nabla \cdot E \underline{v} - \nabla \cdot P \, \underline{v} + \nabla \cdot \lambda \, \underline{\nabla} T + \left\{ \frac{\partial E}{\partial t} \Big|_{chem} \right\} \tag{4}$$

where ρ, $\rho \underline{v}$, E and P are the total mass, momentum, and energy densities and pressure, respectively. The $\{\rho_i\}$ and $\{\underline{V}_i\}$ are the mass density and the diffusion velocities of the individual species. The quantities η and λ represent the viscosity and the thermal conductivity of the gas mixture at specified $\{\rho_i\}$, and temperature, T. The $\{P_i\}$ and $\{L_i\}$ refer to chemical production and loss processes for species i, and the last term in Eq. (4) represents the change in energy due to chemical reactions which is added to the fluid dynamic energy density. This term only enters the total energy equation implicitly and is therefore enclosed in brackets. The model we have used is one-dimensional, and the spatial gradients are evaluated only in the r-direction, where r is a generalized position coordinate. Currently we have assumed Cartesian coordinates for our shock tube simulations but the model allows for other coordinate systems.

4

There are a number of inherent numerical difficulties we face in detailed modeling of the transport of a shock or a flame front in a reacting medium. One problem arises as the result of the widely different time scales characteristic of fluid and chemical processes. Another obstacle to numerical simulation is that conventional numerical methods are unable to resolve accurately the steep gradients in pressure, density, and temperature characteristic of these phenomena. Finally, we face the problem of a time-consuming chemical rate integration which, because of the many species and reactions required to model a realistic system, can increase calculation time by orders of magnitude over a pure fluid calculation.

We approach the time-scale problem by employing the fractional-step method commonly known as time-step splitting. For example, the species density equations are separated into spatial derivative terms and chemical production and loss terms. The resultant set of partial differential equations are solved separately from the set of nonlinear ordinary differential equations at each time step. The solution is a result of coupling the fractional steps, accomplished by providing the initial conditions for one step with the results of the solution from the other step. This technique is advantageous since very efficient and modular computer codes can be produced and the various parts of an equation may be solved with an appropriate time-step. Accuracy is tested by decreasing the time-step and by increasing the resolution, and then checking for variations in the answers.

5

The fluid dynamic equations expressing the conservation of mass, momentum, and energy are solved by the Flux-Corrected Transport (FCT) method,[1,2,3] as are the continuity equations for the densities of the individual molecular species. FCT is designed to reproduce steep gradients particularly well, a situation which occurs fluid dynamically in shocks and chemically in combustion fronts and flames. Furthermore, because negative densities cannot occur using the method, many types of numerical instabilities which plague reactive flow calculations can be avoided without excess non-physical numerical diffusion.

The particular FCT algorithm chosen is a simple variant of the ETBFCT program[3]. Instead of following the cell center locations on the generalized one-dimensional grid and averaging these to define cell boundaries, we follow the cell boundaries as primal quantities and average these locations to define cell centers. By ascribing physical reality to the cell boundaries, numerical diffusion between can be eliminated and Lagrangian treatment of system boundaries is simplified.

An important feature of these FCT algorithms is the lack of an artificial viscosity needed to stabilize shocks. The flux correction procedure itself ensures that the shocks are one or two zones wide and have maximal resolution. Physically correct mass diffusion, viscosity, and thermal conduction terms are included in the model by a separate diffusion subprogram which takes advantage of time-step splitting. The fluid dynamics time integration is performed by an explicit two step predictor-corrector technique[3]. The usual Courant-Friedrich-Lewy

6

stability conditions apply to the hydrodynamics time-step. However the chemistry can proceed on a faster scale provided that the hydrodynamics does not respond to these chemical changes on this faster scale.

Another important feature of the FCT algorithms chosen is their ability to divorce the grid motion from the fluid flow. We have used this freedom to include an efficient adaptive gridding procedure to automatically follow regions such as the shock front, where enhanced resolution is required. In this paper the adaptation is based on the shock. The region immediately around the shock front and for predetermined distances on each side is gridded with finely spaced cells. The fine spacing transitions smoothly into the more coarsely resolved region. As the shock moves along the length of the tube, the finely-spaced region moves with it and reflects off the boundary wall. We have found that the condition on the acceleration,

$$ \left| \frac{\Delta P}{\Delta r} \right| \frac{1}{\bar{\rho}} = \text{maximum}, $$

is adequate for locating the shock front. Here P is the pressure, r is the generalized position coordinate, and $\bar{\rho}$ is the average mass density. In principle there can be any number of finely-spaced regions and the method will also be useful for obtaining the required resolution at a flame front.

The rate equations for the species number densities can be written as a set of first-order, coupled, nonlinear, ordinary differential equations of the following form for the ith species:

7

$$\frac{\partial n_1}{\partial t} = P_i - n_1/\tau_1 , \tag{5}$$

where n_1 is the density, P_1 is the production rate, and τ_1 the characteristic loss time.

The "selected asymptotic method"[4,5] used to solve these equations, determines which equations satisfy an appropriately chosen stiffness criterion. The non-stiff equations are solved by a second order Adams method while a very stable asymptotic method is applied to the stiff equations. This method is particularly suitable for the situation which frequently occurs in the near equilibrium state when the production and loss rates are very large but nearly cancel. Small numerically produced oscillations, which result from short time constants in the kinetics and would produce prohibitively short time steps, are effectively reduced. The time step is carefully monitored to insure the accuracy and convergence of the method. In coupled chemical and hydrodynamic models the accuracy of the chemical integration can be relaxed somewhat due to the presence of unavoidable truncation errors in the fluid dynamics and transport schemes and the uncertainties in the rate constants.

The selected asymptotic method is very efficient for reactive flow problems since it has very low overhead and can be restarted inexpensively. It has been programmed to make efficient use of the parallel processing capability of vector computers.

In the time-splitting approximation, we assume that the fluid motion is frozen while the chemical rate equations are advanced using their own appropriate time-step. At the end of a fluid integration step, the internal energy, ϵ, is obtained by evaluating

$$\epsilon = E - \frac{1}{\rho} \, \rho v^2, \tag{6}$$

where E, ρv, and ρ have been determined. Then the temperature, which is required for evaluation of chemical reaction rates and diffusion coefficients, is found by iterating an equation of the form

$$\epsilon = h \, (T, \, \{n_i\}) - N \, k \, T \tag{7}$$

where ϵ is in ergs/cm^3, h is the enthalpy, $\{n_i\}$ and N are the species and total number density, respectively, and k is Boltzmann's constant. Thus during a chemical integration step, T is found after the equations are solved for $\{n_i\}$. The internal energy of the system is held constant for each chemical time-step. We emphasize that at each time-step the enthalpy and the specific heats are re-evaluated using the new densities and temperature.

The diffusion velocities $\{V_i\}$, are found by solving[16]

$$\sum_{k \neq j} \frac{n_j n_k}{N^2 D_{jk}} \, (V_k - V_j) = \nabla \left(\frac{n_j}{N} \right) \; - \; \left(\frac{\rho_j}{\rho} - \frac{n_j}{N} \right) \frac{\nabla P}{P}$$

$$+ \; \sum_j \frac{n_j n_k}{N^2 D_{jk}} \left(\frac{D_{Tj}}{\rho_j} - \frac{D_{Tk}}{\rho_k} \quad \frac{\nabla T}{T} \right) \tag{8}$$

subject to the constraint

$$\sum_j \rho_j V_j = 0. \qquad (9)$$

The $\{D_{jk}\}$ are binary diffusion coefficients and will be discussed in the next section. The $\{D_{Tj}\}$ are the thermal diffusion coefficients and have been set equal to zero in the calculations presented below. Equations (8) and (9) form a set of linear coupled equations in $\{V_j\}$ which are solved by an iterative technique which will be described in detail in a future paper.

III. Chemical Model

The results presented below are derived from simulations of shocks in a mixture of hydrogen and oxygen which may include an inert species such as argon or helium. This relatively simple combustion system is ideal for our benchmark work because it has been studied extensively in laboratory shock tubes and because a great deal of effort by the combustion community has gone into determining the relevant reaction mechanisms and rates over a wide temperature range[6,7,8,9,10]. For H_2-O_2 combustion, we monitor at each point in the system the evolution in time of the temperature and eight reacting species densities, H_2, O_2, H_2O, H, O, OH, HO_2, and H_2O_2, and the density of the inert material.

There are over forty reaction paths included here which are of varying importance at each temperature and which control the intermediate and final densities. These are summarized in Table I. The main features of the induction and termination periods are fairly well understood. Useful for our purposes is the fact that in the fast reaction region in which we are interested, the major termination paths are through thermolecular reactions and not wall reactions. We are relatively secure in our treatment of termolecular reaction rates, which are properties of the composition of the systems; the wall reactions would vary with the wall coatings and require empirical modeling. In the work presented here, we assume there is one rate coefficient for a termolecular reaction, regardless of what the third body is. There is some information available on the efficiencies of various species, and this can be incorporated in future calculations.[11]

11

The enthalpies for the species we monitor have been taken from the JANAF tables[12] and from the sixth order enthalpy coefficients of Gordon and McBride.[13] For each species we have transformed their values into a seventh order polynomial fit which goes from $0^{\circ}K$ to the maximum temperature given in the JANAF tables. The enthalpy of a species "i" can then be written

$$h^i = \sum_{n=0}^{6} a_n^i \left(\frac{T}{1000}\right)^n \tag{10}$$

where h^i is in units of ergs/cm^3 and T is in degrees Kelvin. The coefficients a_n^i are given in Table II. Our motiviation for using one fit over a wide temperature range instead of table look-ups or different sets of coefficients for the temperature range below and above $1000^{\circ}K$ lies in the speed and ease with which the evaluation of expressions such as Eq.(10) can be vectorized for efficient computation.

The transport processes[14] such as diffusion, thermal conduction, and viscous dissipation are generally slow compared to the fluid flow velocities with which we are concerned in a shock problem and their effects on the reaction zone are predictably small. We have, however, included them in the model for completeness and because this generic model will also be applied to the slower propagation of a flame front. We will comment briefly in the sections below on the size of the diffusion and conductivity effects. The transport coefficients we have chosen are a first approximation. When this model is applied to a propagating flame front, we will try to incorporate more accurate values of the quantities.

Accurate binary diffusion coefficients are given by Marrero and
Mason.[15] These have been used where available. When a coefficient
was not tabulated, we have exploited the similarity between diffusion
of species close in molecular weight to approximate the expression
we need. Table III summarizes the binary diffusion coefficients we
have used.

The thermal conductivity of species "i" is evaluated in terms of
the viscosity, η_i, the ratio of specific heats, γ_i, and the molecular
weight, m_i:

$$\lambda_i = \frac{1}{4} \ (9 \ \gamma_i - 5) \ \frac{8.12 \times 10^7}{(\gamma_i - 1)m_i} \ . \eta_i \qquad (11)$$

The units of λ_i are erg-cm^{-1}-sec^{-1}-$^{\circ}$K^{-1}. This expression reduces to
the usual monatomic gas expression for the appropriate value of γ_i.
Values of η_i, summarized in Table IV, are admittedly only first
approximations.

The conductivity of the gas mixture λ_M, has been evaluated from
an approximate expression of the form:

$$\frac{1}{\lambda_M} \cong \frac{1}{\eta_M} \ \left\{ \frac{1}{N^2} \ \sum_i \ n_i^2 \ \frac{\eta_i}{\lambda_i} \right\} \qquad (12)$$

where the expression for η_M is [14],

$$\eta_M \cong \sum_i \frac{\eta_i^2}{\dfrac{n_i^2}{\eta_i} + \dfrac{1.385 \times 10^6}{m_i N} \sum_{k \neq i} \dfrac{\eta_i \eta_i}{D_{ij}}} \qquad (13)$$

We note that Eq. (10) for λ_M is purely empirical and based on a general-
ization of the two-species empirical formula[14]. After examining
measured values of η_M for many mixtures we decided this expression gives
accurate enough values for the density and temperature ranges with
which we are concerned here.

13

IV. Discussion of Results

We have performed a number of simulations of shocks in an H_2-O_2 medium varying the initial temperatures, pressures and amounts of diluent on the low density, reacting side of the diaphragm. In this section we present calculations of a shock propagating through a reacting gas, initially at room temperature, with no diluent present to absorb heat. Within the constraints of a one-dimensional model, these calculations show how the energy released during the chemical reactions affects the fluid motion.

Figure 1 summarizes the initial conditions before the diaphragm is burst. The driver gas is helium at 10 atm and the low density region is a stoichiometric mixture of H_2 and O_2 at 0.01 atm. Small amounts of the intermediate chain centers, the peroxides, and water have been included on the reacting side. The initial densities of these minor constituents have been determined in a separate calculation by allowing a stoichiometric mixture of H_2 and O_2 to "equilibrate" at fixed temperature (300°K) for about an hour of physical time. The chemical reactions described by the rates in Table I control this process.

Table V gives the solution to an <u>ideal</u> diaphragm-shock problem defined in Fig. 1 and is the analytic solution to the Rankine-Hugoniot equations. These results are strictly valid only when there are no chemical reactions, diffusion, or conductivity in the fluid and when the gas constant is independent of temperature. Therefore Table V can only be used as a guide to understanding the detailed simulation presented below in which chemical reactions, molecular diffusion, thermal conductivity, and the temperature dependence of the specific heats are explicitly included.

14

At the onset of the calculation, the diaphragm is removed and the driver fluid begins to move into the low density region. The five distinct regions described by Table V are not clearly differentiated in our calculations with 0.1 cm zones until $\sim 1\times10^{-5}$ sec. Then we begin to see the clear formation of a shock front, contact discontinuity, and expansion fan. By about 2×10^{-5} sec the fluid flow has settled down and looks very much like the ideal pattern. Until enough time has elapsed so that there are substantial changes in the species densities due to the chemical reactions, the fluid motion is relatively unaffected by chemistry. Detailed comparisons over a wide range of shock parameters during this early time have verified the accuracy of the non-reacting fluid model as compared to the ideal conditions in Table V.[1]

Figure 2a shows the temperature profile after $\sim 1.34\times10^{-4}$ sec. At this time the shock front is located at 40 cm down the tube. The different regions are clearly separated in the calculation and the energy released by chemical reactions has noticeable effects on both the shock speed and the shape of the shocked region. The dashed line marks the corresponding temperature profile for the ideal non-reacting fluid calculation. An increase in the temperature at the back of the shocked region, where most of the chemical reactions have occurred, is clearly visible. The calculation also shows a broadening of the region surrounding the contact discontinuity due to diffusion of the helium driver gas into the reactive mixture. The effect of this temperature decrease is apparent in Figs. 2b, 2c and 3.

Figure 2b shows the total densities corresponding to the temperatures
shown in Fig. 2a. As one might expect, the high temperature regime
corresponds to a low density regime in the shocked region. The total
pressure corresponding to Figs. 2a and 2b is shown in Fig. 2c. We note
that both temperature and total density can vary by as much as a factor
of two in the shocked region, whereas the pressure variation is at most
about 30%. The calculated fluid velocity has not been shown since it
varies at most by 10% from the solutions presented in Table V.

Figure 3 shows the number density of H_2 and O_2, the chain centers,
and the product H_2O as a function of location along the length of the
tube at 1.47×10^{-4} sec. If we were looking at a case where the tempera-
ture were uniform across the high temperature region (i.e., large amounts
of diluent present), we would expect the H_2O peak to be in front of the
OH peak. In such a case the spatial difference between the peaks would
be analogous to the temporal separation between peak OH formation which
precedes the maximum product formation in a homogeneous reacting gas
mixture. Looking for this effect in the highly exothermic case we are
studying can be misleading: here we have to consider both kinetic and
fluid dynamic effects. The high OH densities indicate that combustion
is occurring between about 36 and 38 cm and this is in agreement with
the high temperatures shown in Fig. 2a. The unreacted H_2 and O_2 near
35 cm is in the cool region near the contact discontinuity into which
helium has diffused.

We have used the same numerical model in a slightly different
mode to calculate the reactions in a stationary premixed system over a
range of temperatures. This is done by by-passing the transport part
of the calculation, setting the density across the grid equal to that

16

behind the shock front, and at the onset of the calculation putting a linear temperature ramp across the grid. With no fluid motion and no diffusion processes, this is equivalent to performing a large number of independent time-dependent chemical rate calculations simultaneously.

The difference between highly exothermic chemical reactions occurring behind a moving shock front and reactions in a stationary premixed homogeneous gas is shown in Fig. 4. Using the temperature ramp method described above for the range 1100-1500°K, we have monitored the gas mixture as it is suddenly brought to high temperatures, reacts, and self-consistently heats. Figure 4a shows the self-consistent temperature increase with time. The curves represent stoichiometric H_2-O_2 mixtures with density equal to that immediately behind the shock front. Initially these mixtures are suddenly heated to 1100, 1200, and 1500°K respectively.

The three curves in Fig. 4b show the increases in the H_2O density corresponding to the temperature profiles in Fig. 4a. After an ignition period, the bulk of the water is formed and the curves level off. Also on this figure we have plotted the maximum water density calculated behind the moving shock front as a function of time. Note that the temperature behind the ideal shock is about 1200°K, and the shock results fall between the stationary 1200 and 1300°K curves with respect to ignition times, but below these curves in maximum density values. This latter difference is the natural expansion which occurs when chemical energy is released.

Another striking difference between the homogeneous, premixed and the shock calculations is the difference in maximum temperature attained. Behind the shock this is about 2300-2400°K, whereas the

17

calculations in Fig. 4 show a maximum of about 3200°K. This difference in thermal energy is that energy used to accelerate the shock front.

At this point we note that the calculations show the presence of a temperature oscillation in the shocked region even when there are no chemical reactions permitted. At 1.34×10^{-4} sec, these waves have an amplitude of about 25°K, and they are damped somewhat when thermal conductivity is allowed. These are small, finite amplitude sound waves, a result of initial transients. As the shock region spreads out and time increases, the amplitude of these waves also decrease. The oscillations are primarily in the fluid velocity and this in turn is amplified in the internal energy and the pressure calculation through Eq. (6).

The second problem we shall discuss is that of a shock reflected off of a rigid wall. Many shock tube experiments are designed to take advantage of the relatively uniform regime near the wall behind the reflected shock. The temperature and density are further elevated here and the fluid velocity is essentially zero. Thus there is a period of relative calm that can be used to watch reactions develop.

In order to model the region behind a reflected shock, we have allowed our finely gridded region to move to the wall with the initial shock front. Then the grid motion is restricted so that it does not move backwards. Thus we retain fine resolution near the wall. We look at the same shock as described above and set the wall at 50 cm.

For this problem we present our results a little differently. We assume that there is a "hole" 1 cm from the reflection wall, at 49 cm, and monitor what passes by. Figure 5 shows how the temperature at this location changes as a function of time. When the shock passes 49 cm, the

18

temperature jumps to about 2300°K which in this case is characteristic of the temperature behind the shock after burning. The temperature stays at this value until the reflected shock passes over this position again. Then the temperature increases to about 3500°K and the pressures increase by a factor of about three. These increases are consistent with what is expected from a solution of the jump conditions for an ideal shock reflected from a wall[17].

The calculated fluid velocity behind the reflected shock is not exactly zero. It is several orders of magnitude less than the $\sim 10^{5}$ cm/sec characteristic of the fluid before it is reflected from the wall. As described above, these are finite amplitude sound waves generated in the process of reflection which decrease in amplitude as this region expands.

Once the reflected shock reaches the low temperature region behind the original contact discontinuity, a large amplitude wave will propagate back to the wall and modify the uniform pressure and temperature region. In the case described above, we have a region of low temperature (60°K), high density material (1.6×10^{-4} g/cm^{3}) moving into a region of high temperature (2300°K), and lower density (1.0×10^{-4} g/cm^{3}). For a long shock tube, where the shocked region has spread out over a large distance, there can be a substantial time when the reflected high temperature region persists. Then except for the small finite amplitude sound waves which are present even in experimental situations, the medium can be considered at rest.

19

At each spatial and temporal location along the length of the
tube we can monitor the detailed production and loss rates for each
chemical species. For example, an analysis of the chemical
production and loss rates describing the 35 cm position in Fig. 3
shows that the chemical species are clearly out of chemical equili-
brium. An extensive analysis of the rate scheme will be reserved for
a future paper, in which we will simulate an actual laboratory shock
tube experiment.

V.   Conclusion

In producing the results presented above, a premium has been paid for the complete time-dependent prediction capability. Both the chemical kinetics and the shock hydrodynamics have been treated simultaneously and accurately by explicitly integrating on the appropriate time and space scales. Were we to separate these calculations and ignore the fluid-chemistry interaction, we would arrive at simplified representations which are enlightening but limited quantitatively. If we assumed ideal shock hydrodynamics and did only a single, decoupled kinetics calculation at one given pressure, temperature, and density, we would not resolve the shock acceleration due to combustion shown in Fig. 2. Simple comparisons such as Fig. 4b also illustrate this point. Shock reflection off of a wall is another situation where every point in space has a different chemical and fluid dynamic history. The ideal conditions of zero fluid velocity and constant temperature and pressure are altered by any exothermic reactions taking place.

We have focused our attention on a shock calculation because it represents a severe test of the resolution and accuracy of our numerical model. This is part of an on-going combustion program at NRL to measure, model, and predict the behavior of highly complex, interactive combustion systems. We are currently applying the shock model to data from a shock-initiated deflagration which accelerates and increases the shock pressure[18]. In the future, the model will be used in coordination with shock tube experiments to decipher the details of hydrocarbon fuel reaction rates and induction behavior.

21

ACKNOWLEDGMENTS

Table I

CHEMICAL REACTION RATES[*]

	Reactants	Products	Reaction Rate Constants $k = AT^B e^{C/T}$			Reference
			A	B	C	
1	H + H + M	H_2 + M	1.80(-30)	-1.00	0.00	19
2	H + O + M	OH + M	2.80(-32)	0.00	0.00	20
3	H + OH	H_2 + O	1.40(-14)	1.00	-5.50(+03)	19
4	H + OH + M	H_2O + M	6.20(-26)	-2.00	0.00	19
5	H + H_2O	H_2 + OH	1.50(-10)	0.00	-1.03(+04)	19
6	H + O_2	O + OH	3.70(-10)	0.00	-8.45(+03)	19
7	H + O_2 + M	HO_2 + M	4.10(-33)	0.00	5.00(+02)	19
8	H + HO_2	H_2 + O_2	4.20(-11)	0.00	-3.50(+02)	19
9	H + HO_2	O + H_2O	8.30(-11)	0.00	-5.00(+02)	21
10	H + HO_2	OH + OH	4.20(-10)	0.00	-9.50(+02)	19
11	H + H_2O_2	H_2 + HO_2	2.80(-12)	0.00	-1.90(+03)	19
12	H_2 + O	H + OH	3.00(-14)	1.00	-4.48(+03)	19
13	H_2 + OH	H + H_2O	3.60(-11)	0.00	-2.59(+03)	19
14	H_2 + O_2	H + HO_2	9.10(-11)	0.00	-2.91(+04)	19
15	H_2 + O_2	OH + OH	2.80(-11)	0.00	-2.42(+04)	22
16	H_2 + HO_2	H + H_2O_2	1.20(-12)	0.00	-9.40(+03)	19
17	H_2 + HO_2	OH + H_2O	1.21(-12)	0.00	-9.41(+03)	22
18	H_2 + M	H + H + M	3.70(-10)	0.00	-4.83(+04)	19
19	O + O + M	O_2 + M	5.00(-35)	0.00	9.00(+02)	23
20	O + OH	H + O_2	2.72(-12)	2.80(-01)	8.10(+01)	24,19
21	O + OH + M	HO_2 + M	2.80(-31)	0.00	0.00	24,25

Table I (continuation)

	Reactants	Products	Reaction Rate Constants $k = AT^B e^{C/T}$			Reference
			A	B	C	
22	$O + H_2O$	$H + HO_2$	1.75(-12)	4.50(-01)	-2.84(+04)	24,21
23	$O + H_2O$	$OH + OH$	1.10(-10)	0.00	-9.24(+03)	19
24	$O + HO_2$	$OH + O_2$	8.00(-11)	0.00	-5.00(+02)	26
25	$O + H_2O_2$	$OH + HO_2$	1.40(-12)	0.00	-2.13(+03)	21
26	$OH + OH$	$H + HO_2$	2.00(-11)	0.00	-2.02(+04)	19
27	$OH + OH$	$H_2 + O_2$	1.09(-13)	2.60(-01)	-1.47(+04)	16,24
28	$OH + OH$	$O + H_2O$	1.00(-11)	0.00	-5.50(+02)	19
29	$OH + OH + M$	$H_2O_2 + M$	2.50(-33)	0.00	2.55(+03)	19
30	$OH + HO_2$	$H_2O + O_2$	8.30(-11)	0.00	-5.00(+02)	26
31	$OH + H_2O$	$H_2 + HO_2$	1.34(-14)	4.30(-01)	-3.62(+04)	24,22
32	$OH + O_2$	$HO_2 + O$	2.20(-11)	1.80(-01)	-2.82(+04)	24,26
33	$OH + H_2O_2$	$H_2O + HO_2$	1.70(-11)	0.00	-9.10(+02)	19
34	$OH + M$	$H + O + M$	2.20(-08)	3.00(-02)	-5.14(+04)	24,20
35	$H_2O + O_2$	$OH + HO_2$	2.38(-10)	1.70 (-01)	-3.69(+04)	24,26
36	$H_2O + HO_2$	$OH + H_2O_2$	4.70(-11)	0.00	-1.65(+04)	19
37	$H_2O + M$	$H + OH + M$	5.80(-09)	0.00	-5.29(+04)	19
38	$O_2 + H_2O_2$	$HO_2 + HO_2$	1.20(-13)	5.00(-01)	-2.11(+04)	25
39	$O_2 + M$	$O + O + M$	3.00(-06)	-1.00	-5.94(+04)	23
40	$HO_2 + HO_2$	$O_2 + H_2O_2$	3.00(-11)	0.00	-5.00(+02)	21
41	$HO_2 + M$	$H + O_2 + M$	3.50(-09)	0.00	-2.30(+04)	19
42	$HO_2 + M$	$O + OH + M$	1.13(-04)	-4.30(-01)	-3.22(+04)	24,25
43	$H_2O_2 + M$	$OH + OH + M$	2.00(-07)	0.00	-2.29(+04)	19

* Rate Constants are given in units of cm^3/sec, T in $°K$.
Three body rates are in cm^6/sec where M is the third body.
Read 1.80(-30) as 1.80×10^{-30}.

Table II

Enthalpy Coefficients: $h^i = \sum a_n^i \left(\frac{T}{1000}\right)^n$ ergs/cm^3

$$a_n^i$$

Species	n = 0	1	2	3	4	5	6
H	-1.469(-17)	3.?50(-13)	7.092(-16)	-5.880(-16)	2.016(-16)	-3.095(-17)	1.761(-18)
H$_2$	1.192(-15)	4.745(-13)	-1.200(-14)	2.665(-14)	-7.773(-15)	1.002(-15)	-4.897(-17)
O	3.634(-16)	3.790(-13)	-3.246(-14)	1.545(-14)	-3.893(-15)	5.050(-16)	-2.59(-17)
OH	2.115(-14)	4.835(-13)	-4.124(-14)	5.310(-14)	-1.711(-14)	2.408(-15)	-1.269(-16)
H$_2$O	3.377(-15)	5.129(-13)	5.887(-14)	3.522(-14)	-1.499(-14)	2.224(-15)	-1.179(-16)
O$_2$	2.480(-15)	4.413(-13)	1.063(-13)	-3.522(-14)	7.910(-15)	-9.162(-16)	4.272(-17)
HO$_2$	4.125(-15)	4.702(-13)	2.434(-15)	-7.140(-14)	1.224(-14)	-1.127(-15)	4.295(-17)
H$_2$O$_2$	-1.595(-16)	5.752(-13)	-2.320(-13)	1.712-(-12)	-2.162(-12)	1.177(-12)	-2.393(-13)
Inert	0.0	3.450(-13)	0.0	0.0	0.0	0.0	0.0

Read 3.450(-13) as 3.450 $\times$ 10^{-13}

T = temperature in °K.

(Numbers in tables refer to coefficients in key below)

	H	H_2	He	O	OH	H_2O	O_2	HO_2	H_2O_2
H		1	6	2	2	2	3	3	3
H_2			8	2	2	2	3	3	3
He				2	2	2	4	3	3
O					2	7	5	5	5
OH						7	5	5	5
H_2O							5	5	5
O_2								7	7
HO_2									7

Key

1. $8.2 \times 10^{16} \, T^{.728}/N \quad cm^2/sec$

2. $3.40 \times 10^{17} \, T^{.749}/N$

3. $3.0 \times 10^{17} \, T^{.732}/N$

4. $3.4 \times 10^{16} \, T^{.749}/N$

5. $9.6 \times 10^{16} \, T^{.774}/N$

6. $1.0 \times 10^{18} \, T^{.732}/N$

7. $8.2 \times 10^{16} \, T^{.724}/N$

8. $1.0 \times 10^{18} \, T^{.732}/N$

N = total number density

T = temperature in $^\circ K$

Table IV

Viscosities, η [14]

Species	η ($^g/cm\text{-}sec$)
H	$3.95 \times 10^{-6} \ T^{\frac{1}{2}}$
H_2	$4.71 \times 10^{-6} \ T^{\frac{1}{2}}$
He	$7.66 \times 10^{-6} \ T^{\frac{1}{2}}$
O	$1.15 \times 10^{-5} \ T^{\frac{1}{2}}$
OH	$1.10 \times 10^{-5} \ T^{\frac{1}{2}}$
H_2O	$1.60 \times 10^{-5} \ T^{\frac{1}{2}}$
O_2	$1.16 \times 10^{-5} \ T^{\frac{1}{2}}$
HO_2	$1.16 \times 10^{-5} \ T^{\frac{1}{2}}$
H_2O_2	$1.16 \times 10^{-5} \ T^{\frac{1}{2}}$

T = temperature in $^\circ K$.

Table V

Ideal Shock Solution

Region	1	2	3	4	5
Pressure (dynes/cm^2)	1.056×10^7		1.951×10^5	1.951×10^5	1.056×10^4
Density (g/cm^3)	1.076×10^{-3}		1.557×10^{-4}	2.314×10^{-5}	5.118×10^{-6}
Velocity /cm/sec)	0.0		1.675×10^5	1.675×10^5	0.0
Temperature ($^{\circ}$K)	300	RAREFACTION	60.3	1216	300.0
Sound Speed(cm/sec)	1.016×10^5		4.571×10^4	1.089×10^5	5.388×10^4
Molecular Weight (amu)	4.0		4.00	12.0	12.0
Gamma	1.667		1.667	1.40	1.40

Shock front velocity	2.051×10^5 cm/sec
Contact discontinuity velocity	1.675×10^5
Rarefaction foot velocity	1.218×10^5
Rarefaction front velocity	-1.016×10^5
Mach number	4.00

References

1. Boris, J. P. and Book, D. L., Methods in Computational Physics, Vol. 16, p. 85-129, Academic Press, 1976.

2. Boris, J. P., Computer Physics Communications, 12, 67 (1976).

3. Boris, J. P., Flux-Corrected Transport Modules for Solving Generalized Continuity Equations, Naval Research Laboratory Memorandum Report No. 3237, March 1976.

4. Young, T. R. and Boris, J. P., DNA 1973 Atmospheric Effects Symposium, Vol. 4, DNA Report No. 3131 p-9 (VI 75-442), p. 571, 1973.

5. Young, T. R. and Boris, J. P., J. Phys. Chem., 81, 2424 (1977).

6. Getzinger, R. W. and Schott, G. L., Shock Tube Studies of the Hydrogen Oxygen Reaction System, Physical Chemistry of Fast Reactions, Vol. I Gas Phase Reactions of Small Molecules, B. P. Levitt, Editor, Plenum Press, 1973.

7. Bauer, S. H., Schott, G. L. and Duff, R. E., J. Chem. Phys. 28, 1089 (1958).

8. Skinner, Gordon B. and Gorden H. Rengrose, J. Chem. Phys., 43, 4129, 1965.

9. Ripley, D. L., and Gardiner, Jr., W. C., J. Chem. Phys. 44, 2285 (1966).

10. Gutman, D., Lutz, R. W., Jacobs, N. F., Hardwidge, E. A., and Schott, G. L., J. Chem. Phys. 48, 5689 (1968).

11. Gelinas, R. J., Methane Combustion Kinetics, Science Applications, Inc., Report SAI/PL-NI-77-02, 1977.

12. Stull, D. R. and Prophet, H., JANAF Thermochemical Tables, 2nd edition, Nat. Stand. Ref. Data Ser., Nat. Bur. Stand., No. 37, June 1971.

13. Gordon, S. and McBride, B. J., Computer Program for Calculation of Complex Chemical Equilibrium Compositions, Rocket Performance, Incident and Reflected Shocks, and Chapman-Jouguet Defonations, NASA SP-273, 1976.

14. Hirschfelder, J. O., Curtiss, C. F. and Bird, R. B., Molecular Theory of Gases and Liquids, John Wiley and Sons, 1954.

15. Marrero, T. R. and Mason, E. A., Journal of Physical and Chemistry Reference Data, $\underline{1}$, 3 (1972).

16. Williams, F. A., Combustion Theory, p. 419, Addison-Wesley Publishing Co., Inc., 1965.

17. Bradley, J. N., Shock Waves in Chemistry and Physics, John Wiley and Sons, Inc., 1962.

18. Skinner, G. B., Mueller, G., Grimm, V., and Scheller, K., Combustion and Flame, $\underline{12}$, 436 (1968).

19. Baulch, D. L., Drysdale, D. D., Horne, D.G., and Lloyd, A. C., Evaluated Kinetic Data for High Temperature Reactions, Vol. 1, Butterworths, 1972.

20. Moretti, G., AIAA Journal $\underline{3}$, 223 (1965).

21. Hampson, R. F., and Garvin, D., Chemical Kinetic and Photochemical Data for Modeling Atmospheric Chemistry, NBS Technical Note 866, U.S. Department of Commerce/National Bureau of Standards, Washington, D.C., 1975.

22. Olson, D. B. and Gardiner, W. C., <u>An Evaluation of Methane</u>
     <u>Combustion Mechanisms</u>. Paper presented at the 173rd National
     Meeting of the American Chemical Society, New Orleans, La.,
     March, 1977.

23. Baulch, D. L., Drysdale, D. D., Horne, D. G., and Lloyd, A. C.,
     Evaluated Kinetic Data for High Temperature Reactions, Vol. 3,
     Butterworth, 1977.

24. Engleman, V. S., <u>Survey and Evaluation of Kinetic Data on</u>
     <u>Reactions in Methane/Air Combustion</u>, EPA-600/2-76-003, U.S.E.P.A.
     Office of Research and Development, Washington, D.C., 20460,
     January 1976.

25. Bahn, G. S., Reaction Rate Compilation for the H-O-N System,
     Gordon and Breach, New York, 1968.

26. Lloyd, A. C., Int. J. Chem. Kinetics $\underline{6}$, 169 (1974).
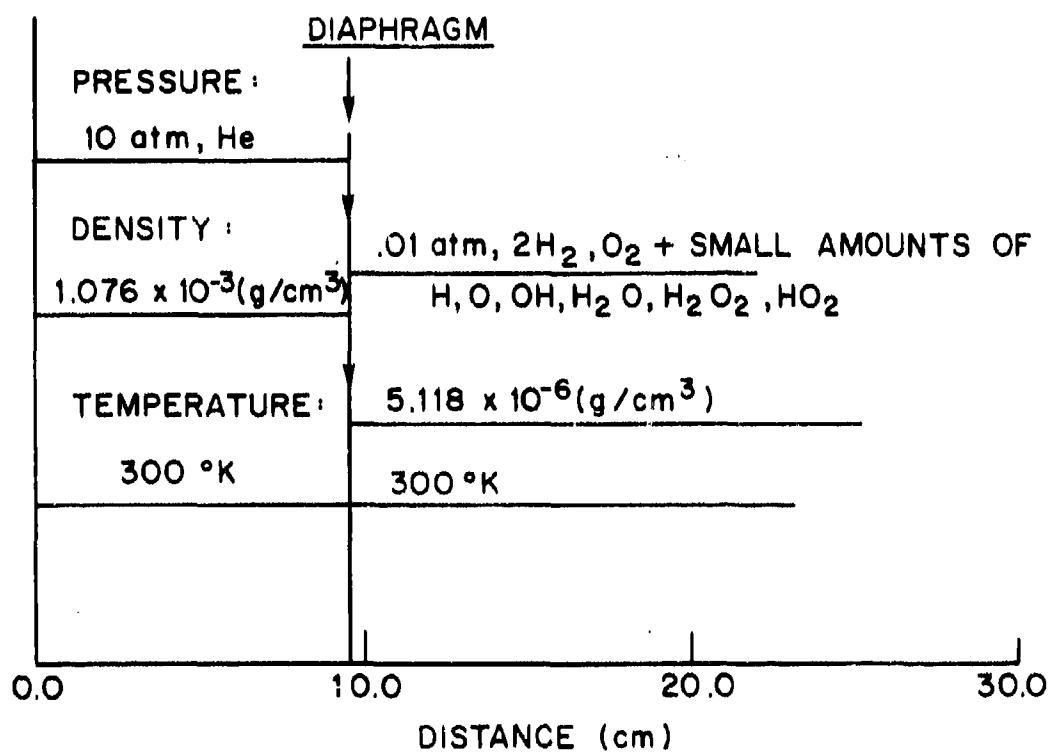
Fig. 1 — Initial density, temperature, and pressure for the
reactive shock calculation
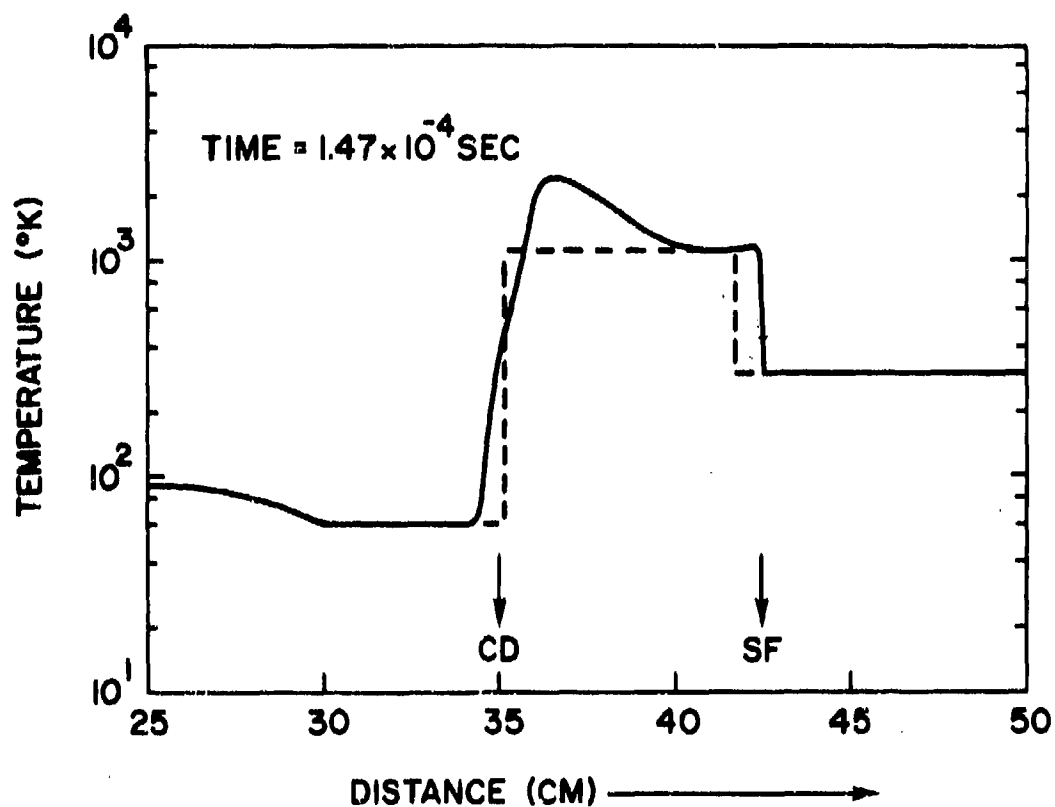
Fig. 2a — Calculated temperature as a function of distance after the shock has traveled 40 cm down the tube. The dashed lines indicate results from the ideal solution. The position of the shock front and contact discontinuity are noted by SF and CD, respectively.
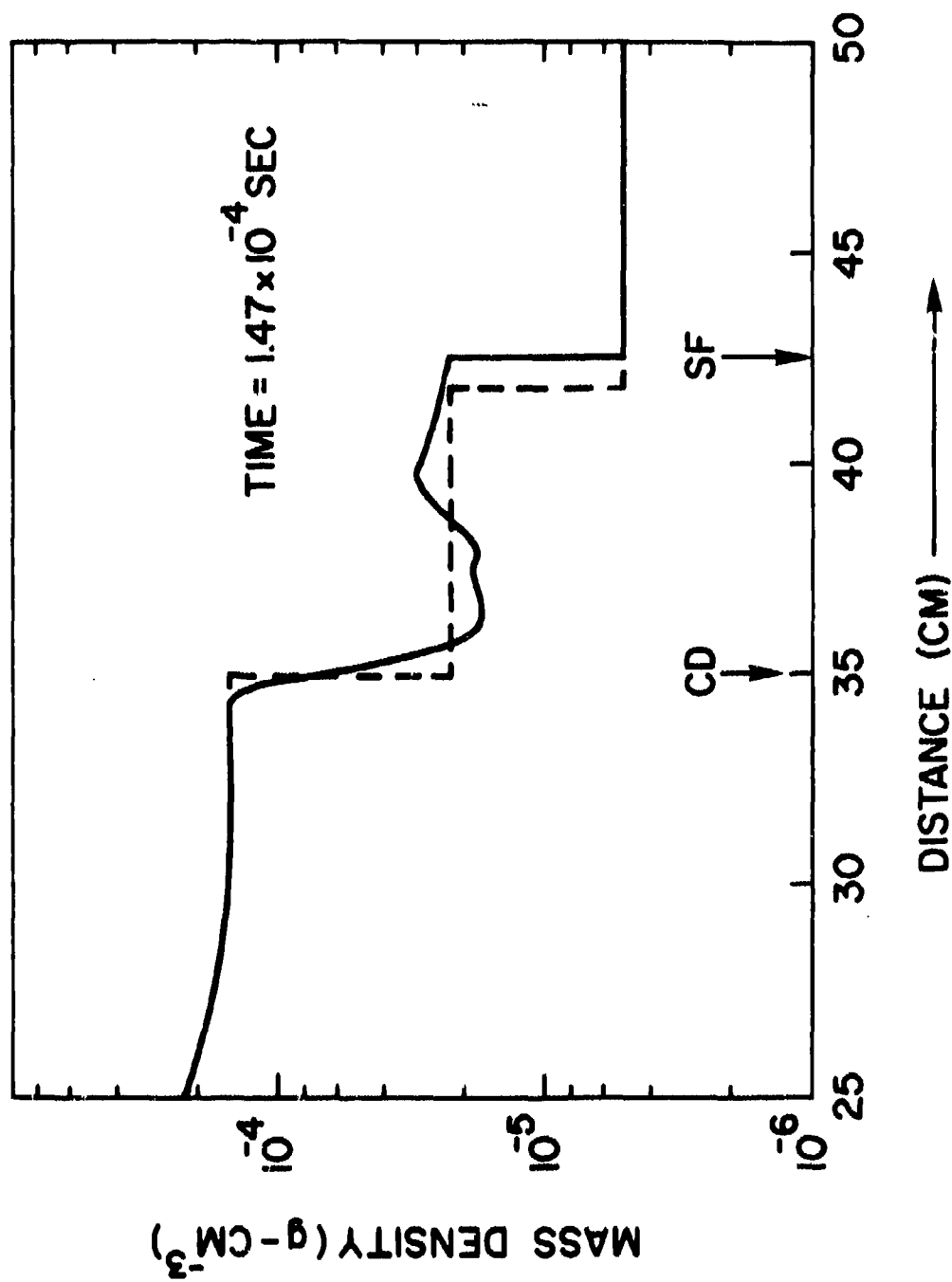
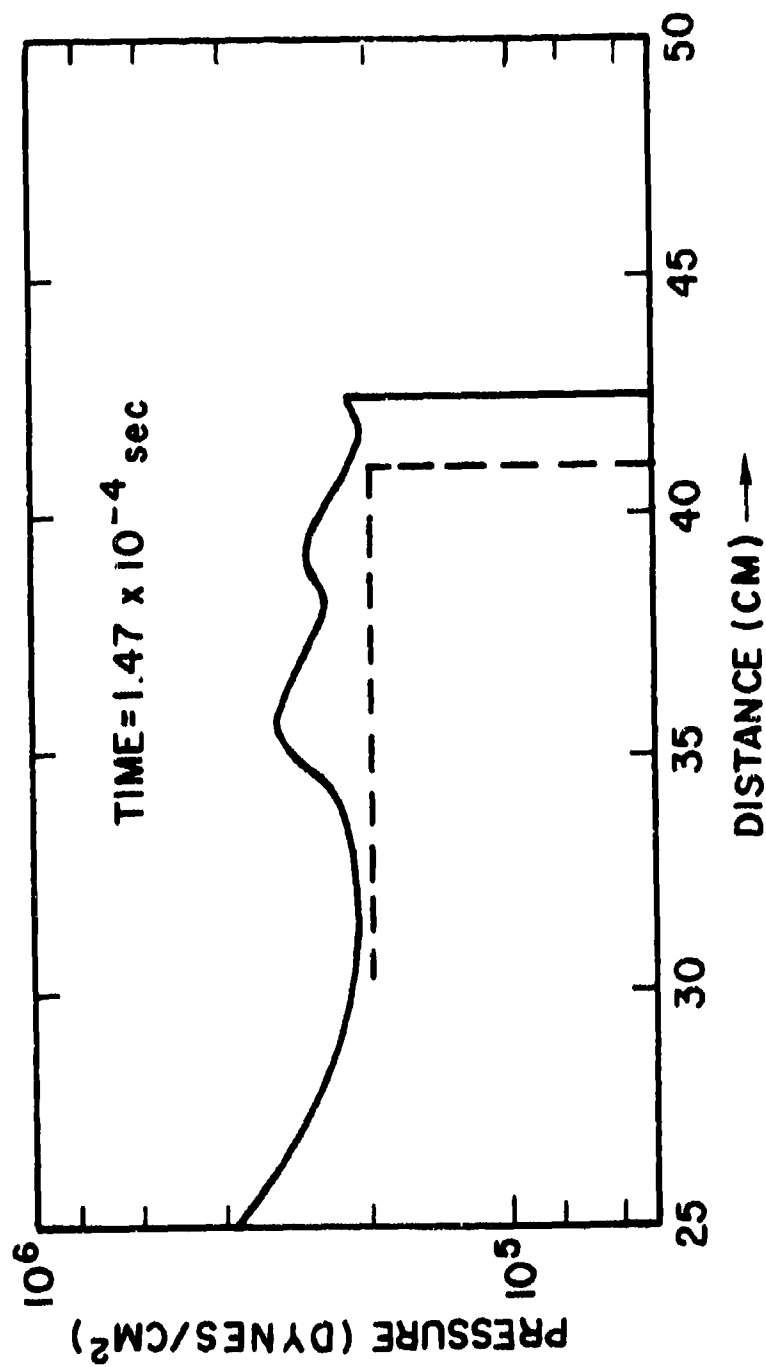Fig. 2b — Calculated mass density as a function of distance at the time corresponding to Fig. 2a

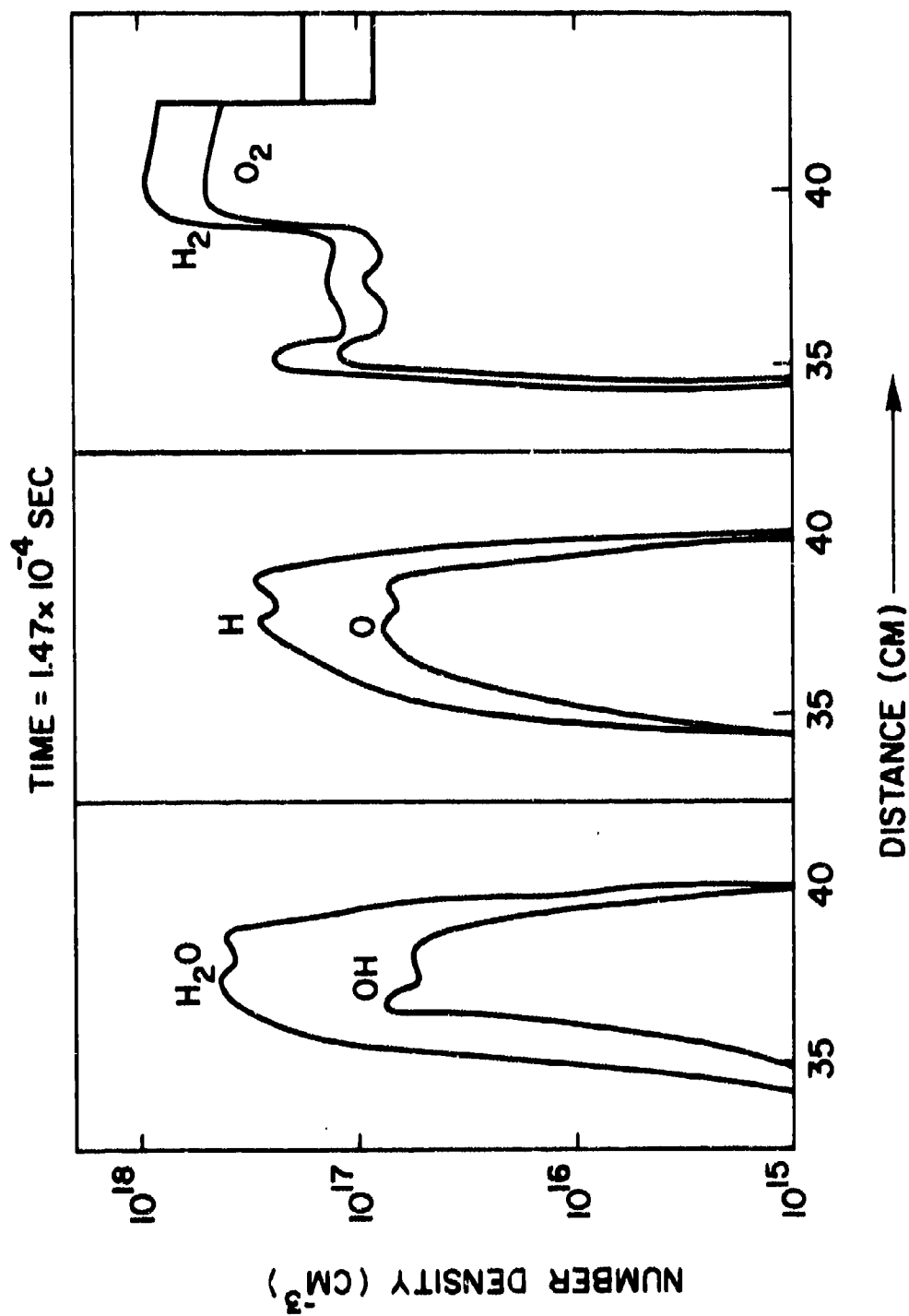Fig. 2c — Calculated pressure as a function of distance at the time corresponding to Fig. 2a

Fig. 3 — Profiles of number density for H_2O, H, O, OH, H_2O, and O_2 as a function of position in the shock tube. These correspond to the temperature profile in Figure 2.
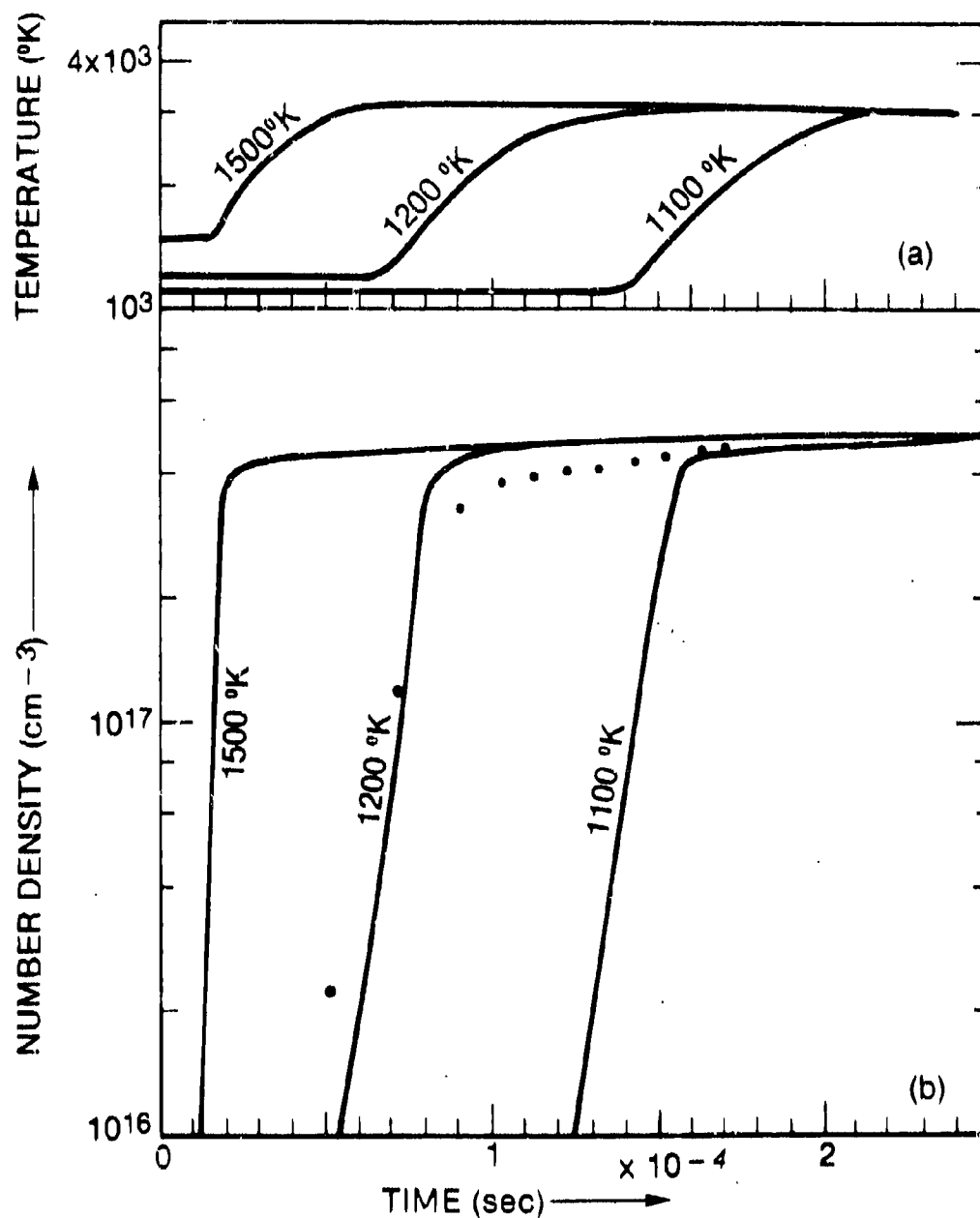
Fig. 4 — (a) Calculation of temperature change as a function of time in a pre-mixed homogeneous $H_2 \cdot O_2$ mixture whose temperature is suddenly raised to 1100 (A), 1200 (B), 1500 (C) °K, (b) the curves show water density as a function of time corresponding to the curves in Fig. 4a. The black dots are the maximum water density calculated behind the moving shock front.
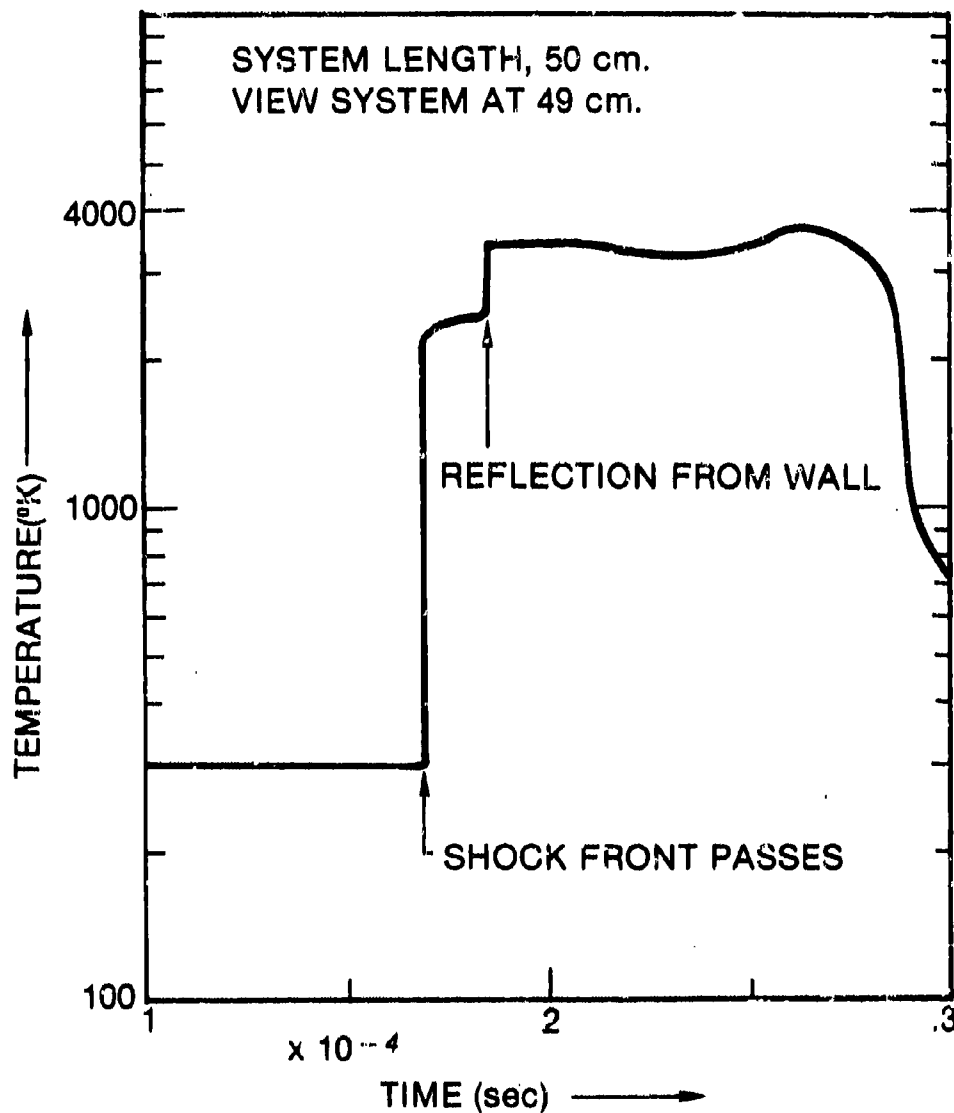
Fig. 5 — Calculations of temperature as a function of time at 49 cm. The shock is reflected at a rigid wall at 50 cm.